Ultrasound in Med. & Biol., Vol. ■, No. ■, pp. 1–9, 2013

0301-5629/$ - see front matter

http://dx.doi.org/10.1016/j.ultrasmedbio.2013.06.007

● *Original Contribution*

ANALYSIS OF ULTRASONIC WAVES PROPAGATING IN A BONE PLATE OVER A WATER HALF-SPACE WITH AND WITHOUT OVERLYING SOFT TISSUE

THO N. H. T. TRAN,* LAUREN STIEGLITZ,† YU J. GU,† and LAWRENCE H. LE*†

*Department of Radiology and Diagnostic Imaging, University of Alberta, Edmonton, Alberta, Canada; and †Department of Physics, University of Alberta, Edmonton, Alberta, Canada

(*Received* 29 *June* 2011; *revised* 10 *June* 2013; *in final form* 11 *June* 2013)

Abstract—Recent *in vitro* studies have shown that guided waves can characterize bone properties. However, for clinical applications to be viable, the soft-tissue layer should be considered. This study examined the effect of soft tissue on guided waves using a bovine bone plate over a water half-space and overlaid by a 4-mm gelatin-based soft-tissue mimic. The data (with and without soft tissue) clearly show a high-frequency, fast-propagating wave packet and a low-frequency, delayed phase group. The presence of soft tissue attenuates the signals significantly and increases mode density and number as predicted by theory. The data retain higher frequency content than the bone-plate data at large offsets. Using theoretical dispersion curves, the guided modes can be identified with mode 1 (similar to the *A*0 Lamb mode) minimally affected by the addition of soft tissue. There is infiltration of high-frequency, late-arriving energy within the low-velocity guided-wave regime. Results of travel-time calculation suggest that *P*-wave and *PP*-reflections/multiples within the soft tissue may be responsible for the high-frequency oscillations. (E-mail: lawrence.le@ualberta.ca)

Key Words: **Ultrasound, Guided waves, Osteoporosis, Soft tissue, Cortical bone, Axial transmission, Dispersion, Attenuation.**

INTRODUCTION

Osteoporosis is a serious medical condition affecting more than 200 million people worldwide (Reginster and Burlet 2006). This "silent epidemic" (Njeh et al. 1997; Werner 2004) can be characterized by low bone density and deterioration of bone micro-architecture, resulting in changes to the mechanical properties of bone (Werner 2004). Early detection and monitoring of osteoporosis mainly rely on dual-energy X-ray absorptiometry, though in recent years quantitative ultrasound (QUS) has gained attention for its ability to detect bone fragility (Laugier 2006). Although X-ray absorptiometry is successful in measuring bone mineral density, it cannot determine bone micro-structures and elasticity, which are important determinants of bone strength (Laugier 2006; Moilanen 2008). In comparison, QUS is lower cost, more portable, and does not involve ionizing radiation. Additionally, QUS uses mechanical waves that are more sensitive to the physical properties of bone (*e.g.,* elasticity, absorption, cortical thickness, micro-architecture, density) than absorptiometry (Muller et al. 2005).

The measurement of the mechanical properties of long bone is typically performed along the long axis of a bone sample using the axial transmission method (Bossy et al. 2004b; Le et al. 2010; Lowet and der Perre 1996; Moilanen 2008; Ta et al. 2009; Tatarinov et al. 2005). The axial transmission technique was first developed over 40 years ago for fracture monitoring (Gerlanc et al. 1975; Siegel et al. 1958). By positioning the transmitting and receiving transducers rectilinearly on the same surface of the bone sample, ultrasound travels from the transmitter to the receiver along the long axis of the bone. During measurement, the transmitter is stationary while the receiver is moved incrementally away from it. This acquisition design is effective in analyzing bulk (or body) wave arrivals at short source-receiver distances or offsets (Le et al. 2010) and energetic guided waves at large source-receiver offsets (Lefebvre et al. 2002; Moilanen et al. 2006; Nicholson et al. 2002; Ta et al. 2006). Despite difficulties in mode identification and analysis, guided

Address correspondence to: Lawrence H. Le, Department of Radiology and Diagnostic Imaging, University of Alberta, WMC 2C2.09, 8440 112 St, Edmonton, Alberta, Canada T6G 2B7. E-mail: lawrence.le@ualberta.ca

waves are very useful in determining material properties of long bones (Moilanen et al. 2006; Ta et al. 2006).

Guided waves are generated by the superposition of reflected and mode-converted compressional (*P*) and shear (*S*) bulk waves within a layer bounded by strong reflecting surfaces (Rose 1999; Viktorov 1967). Because of the constructive interference of multiple reflections within the cortex, the resulting guided waves are capable of traveling long distances and interacting with a large portion of the bone sample. Guided waves propagate in multiple modes, each with a phase velocity dependent on frequency, and are sensitive to the boundaries, structure and thickness of the bone sample (Lee and Yoon 2004; Rose 1999; Vavva et al. 2008).

One challenge in the analysis of guided waves is the presence of soft tissue. Because guided waves are sensitive to cortical boundaries, the soft-tissue layer can affect mode generation and alter the dispersive characteristics of guided modes (Moilanen 2008). Furthermore, ultrasound propagates in soft tissue with a velocity that overlaps the velocity of low-order guided modes such as *A*0 Lamb mode in bones and might, therefore, cause phase misidentification (Lee and Yoon 2004; Moilanen et al. 2006). This misinterpretation is possible in a time-distance (*t*-*x*) plot when the *A*0 phase overlaps with the *P*-direct wave within the soft tissue. Attenuation associated with the soft-tissue layer could also lower the signal-to-noise ratio, and hence the clarity of both bulk and guided waves.

Only a few studies have systematically analyzed soft tissue effects, and those that do either resort to theoretical modeling (Moilanen et al. 2008; Vavva et al. 2008) or assume that soft tissue can be simulated by water (Bossy et al. 2004b; Lee and Yoon 2004; Lowet and der Perre 1996; Moilanen et al. 2006). In the latter case, soft tissue over bone is often modeled as a fluid-solid bilayer, because the acoustic properties of soft tissues are similar to those of water. Early work demonstrated how the presence of soft tissue affected velocity measurement of cortical bones. Lowet and der Perre (1996) reasoned that a soft-tissue layer of constant thickness would introduce a constant lag in the transmission time of a lateral wave (head wave) propagating through the underlying cortex. For a soft-tissue layer of nonuniform thickness, Bossy et al. (2004a) used a bidirectional approach to obtain an unbiased estimate of the cortical bone velocity. Moilanen et al. (2006) used water as a soft-tissue phantom to explore the difference between free and immersed aluminium and acrylic plates. They successfully identified the fundamental *A*0 plate mode and bilayer modes, and determined the plate thickness. A bilayered fluid-solid tube model was later introduced (Moilanen et al. 2008) to interpret *in vivo* data. Recently Chen et al. (2012) investigated a bone-mimicking plate coated respectively with a layer of water, glycerol or silicon rubber to study influences of soft tissue on guided-wave propagation. Their findings indicated that the soft tissue–mimicking layer introduced additional guided modes and the soft-tissue/bone dispersive characteristics could be modeled by two independent fluid and solid waveguides. Zhao et al. (2012) studied the guided waves in porcine bone samples covered by a 5-mm soft coating layer. Their results suggested that the fundamental flexural guided wave could be excited and detected using photo-acoustic quantitative ultrasound in the coated bone samples. Nevertheless, their work was limited to the analysis of the *A*0-like Lamb mode only. The aforementioned efforts have provided valuable insights into the complexities of *in vivo* measurements in the presence of soft tissue, though more work is needed to quantify and validate the effect of soft tissue on the excitation and characteristics of guided modes.

To model soft tissue, we synthesized a soft-tissue mimic that has similar properties to human soft tissue. The objective of the present study was to explore the effect of this soft-tissue mimic on the propagation of ultrasound in a cortical bone plate. We combined experimental measurements on a bone plate (with and without a soft-tissue proxy) with analyses of travel times, spectral decomposition, and dispersion characteristics to analyze the data. The findings of guided-wave propagation and mode excitation were further validated by theoretical dispersion curves based on stratified layers. The work reported here was different from the study by Chen et al. (2012) and other studies in some of the following aspects. First, we used a bovine bone plate instead of bone mimics. Second, we used a solid soft-tissue material with ultrasonic properties very close to those of soft tissue. In addition, we placed a water half-space below the bone plate to mimic marrow material. The first three aspects ensured that the properties of the sample resembled closely those of the real bone. We used a bone plate instead of a long bone sample to avoid cylindrical guided waves, which might have complicated the analysis. Moreover, we used the conventional ultrasound method instead of a photo-acoustic technique (Zhao et al. 2012) to excite guided waves. Finally, instead of analyzing the wave modes using the independent fluid and solid characteristic equations (Chen et al. 2012), we used the coupled soft-tissue/bone system and thus the dispersion equation to identify guided modes.

EXPERIMENTAL MEASUREMENTS

Bone phantom

A fresh bovine femur was acquired from a local butcher shop. The residual soft tissue and marrow were removed to allow the bone to be preserved, and the femur was cleaned. Both ends of the bone were removed using

a band saw to minimize potential waveform complications. The bone was further cut along the long axis and the flat top piece was reserved to make a bone plate of dimensions 230 mm (length), 50 mm (width) and 7 mm (mean thickness).

Following the procedure described by Madsen et al. (1978), we fabricated a tissue-like material to mimic human soft tissue using distilled water, food gelatin (Knox), and graphite powder (General Pencil Company, Inc., Redwood City, CA, USA). Initially, 500 mL distilled water was heated to boiling and then 77 g of gelatin powder was added to the water while stirring. After the gelatin was dissolved, 3 g of graphite powder was mixed into the solution. The concentration of suspending graphite particles determined the amount of ultrasonic scattering generated in the material and thus the magnitude of attenuation coefficient. The final hot mixture was allowed to cool enough to touch and then poured on top of the bovine bone plate to form a 4-mm layer of soft tissue overlying the bone surface (Fig. 1). The synthetic gelatin-based material has similar properties to those of human soft tissue (Culjat et al. 2010). The soft-tissue mimic has an approximate attenuation of 0.4 dB/cm around 1 MHz (vs. $\alpha_{\text{soft tissue}} = 0.54$ dB/cm/MHz), a measured density of 1180 kg/m^3 (vs. $\rho_{\text{soft tissue}} = 1043$ kg/m^3), compressional wave velocity of 1556 m/s (vs. $v_{\text{soft tissue}} = 1561$ m/s), and a very slow shear wave speed measured around 20 m/s, consistent in magnitude with the values for soft tissues published in literature (Frizzell et al. 1976; Madsen et al. 1983; Zhang et al. 2007). We used water in place of marrow; water has properties very similar to those of marrow ($v_{\text{water}} = 1480$ m/s vs. $v_{\text{marrow}} = 1435$ m/s) and is often used as a marrow mimic (Culjat et al. 2010).

Experimental procedures

The bone plate was placed on two pairs of rubber corks in a small water tank. The corks were 3.5 cm long with a 4-cm diameter. The water level reached just below the surface of the bone plate so that the bone was not submerged; care was taken to ensure that no air bubbles were trapped underneath the bone plate. The 7-cm-deep water acted as the marrow half-space. Experiments were performed at room temperature, 21°C. Following Le et al. (2010), two 1-MHz angle beam compressional wave transducers (Panametrics C548, Olympus NDT, Waltham, MA, USA) were attached to two angle wedges (Panametrics ABWM-7T-30); one transducer acted as a stationary transmitter and the other as a receiver. The transducer-wedge systems were deployed linearly on the same side of the bone plate (see Fig. 1). Two steel bars provided constant pressure to the transducer-wedge systems against the bone surface during acquisition. A thin layer of ultrasonic gel (Aquasonic 100, Parker Laboratories, Inc., Fairfield, NJ, USA) was applied between the contacting surfaces to ensure good coupling. The transmitter was pulsed by a Panametrics 5800 PR. The signals detected by the receiver were digitized by and displayed on a 200-MHz digital storage oscilloscope (LeCroy 422 WaveSurfer, Teledyne LeCroy, Chestnut Ridge, NY, USA). In the experiment, the receiver started at an offset of 35 mm and was moved away at an increment of 1 mm to a final offset of 98 mm for a total of 64 ultrasound records. Far-offset measurements are important to allow for the buildup of strong guided-wave energy and to minimize the interference of bulk waves with the late-arriving guided waves. Each record was averaged 16 times during acquisition to increase the signal-to-noise ratio and was decimated to 1000 samples with a sampling interval of 0.1 μs.

Fig. 1. The experimental setup for the bone plate (BP) and soft tissue/bone plate (STBP) measurements. Shown here is the STBP sample. Some soft-tissue material was scraped off at the end to show the bone plate. Water below the bone plate is used to mimic marrow. A Canadian 25-cent coin (23.8 mm in diameter) is used to show scale.

The previously described BP procedure was repeated for the soft-tissue/bone plate (STBP) to obtain 64 ultrasound records. The records were stored in a time-distance matrix of amplitudes.

SIGNAL PROCESSING

Phase velocity versus frequency map

To explore the dispersive properties of the bone sample, we first applied a low-pass filter to eliminate wavenumber and frequency components larger than the corresponding Nyquist limits, and then mapped the data to the frequency-wavenumber (f-k) space (Alleyne and Cawley 1991) using a two-dimensional (2-D) Fourier transform. The resulting f-k signals were subsequently transformed into the frequency-phase velocity (f-c_p) domain using the relation $c_p = 2\pi f/k$.

Spectral decomposition

The ultrasound records indicated that the signals were non-stationary and the frequency distribution varied

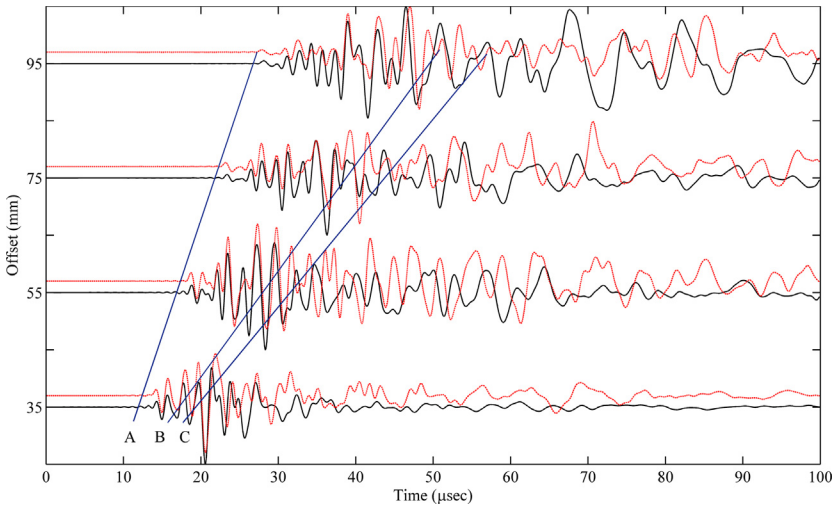

Fig. 2. The time records of the BP (*black solid curve*) and STBP (*red dashed curve*) for close, mid, and far offsets. The STBP records have been time-shifted to align with the BP records using the FAS of the records. Superimposed are the traveling times of the arrivals within the soft tissue. These include the compressional lateral wave traveling as compressional wave (*P*) within the soft tissue and horizontally as *P* in bone (A), lateral wave traveling as *P* within the soft tissue and horizontally as *S* in bone (B), and direct *P* wave in soft tissue (C). The arrival time of the reflection *PP* within the soft tissue is very close to C.

with time. For this reason, we used time-frequency (*t-f*) analysis, or spectral decomposition, of the time-domain signals to quantify the time-sensitive spectral energy variations. Although the *t-f* map provided useful temporal information about pulse-broadening and dispersion of the propagating wave modes, it was particularly useful in separating modes of different frequencies arriving closely in time (Prosser et al. 1999; Xu et al. 2010). We used a multi-wavelet spectral decomposition method developed by Bonar and Sacchi (2010). The idea was as follows: When an incident ultrasound signal reflects on an interface with an impedance contrast, the reflected wavelet is considered a convolution of the incident wavelet with the reflectivity of the interface. Conversely, a reflectivity function is obtained by deconvolving the source wavelet from the reflected signal. For multi-wavelet decomposition, an ultrasound time series is treated as a convolution of the reflectivity function with a dictionary of Ricker wavelets of various frequencies. A Ricker wavelet is uniquely defined by its center frequency (Ryan 1994). Bonar and Sacchi (2010) used complex Ricker wavelets to obtain phase information. The ultrasound signal is deconvolved into a frequency-dependent reflectivity function in time, which can be translated to a *t-f* map. The decomposition problem was posed as an inverse problem with a l_1 norm regularization term to increase sparsity in the solution, and a l_2 norm cost function to fit the data. The joint l_1 and l_2 norm strategy was used to improve the resolution of the decomposition.

RESULTS

Four pairs of ultrasound time records are displayed in Figure 2 for close, mid, and far offsets. Bandpass filtering removed frequencies above 1 MHz and each record was self-normalized for plotting. By self-normalization, each record was divided by its own maximum absolute amplitude. Before normalization, the maximum displacements of the STBP data were significantly smaller (33%) than those of the BP data. Because of the transit time in the transducer wedges, all estimated traveling times were delayed by approximately 5 μs. The first arriving signal (FAS) in BP was consistent with the direct compressional wave traveling through the bone sample from the transmitter to the receivers. When a soft-tissue layer was introduced, the delayed FAS (indicated by line A in Fig. 2) was consistent with a horizontally propagating compressional wave through bone plate. The FAS in the present study was the lateral compressional wave traveling through the soft tissue and along the bone plate. For a better comparison between the BP and STBP data, we aligned the two data sets using the FAS as shown in the figure. Both data sets indicated two wave packets with distinct dominant frequencies and speeds. The early-arriving signals traveled faster with larger phase velocities (*i.e.,* $\Delta x/\Delta t$) and had shorter periods (higher frequencies). These were the non-dispersive bulk reflection arrivals in the layers and both data sets indicated similar bulk wave characters at early times. The late coming signals were of longer periods (lower frequencies), dispersive and exhibited slower

phase velocities. These were the surface or guided waves; the waveforms were quite different for the BP and STBP data because of the influence of the overlying soft tissue.

The self-normalized amplitude spectra for the two cases indicated a mixture of low and high amplitude peaks up to 1 MHz (Fig. 3). At 35 mm offset (see Fig. 3a), the BP spectrum peaked near 0.53 MHz, which was nearly identical to the case of STBP (∼0.49 MHz). As offset increased, most of the ultrasound energy was removed by the attenuation mechanism of the BP or STBP plate and, as such, the dominant peaks shifted toward lower frequency. At 95 mm (see Fig. 3b), the BP spectrum remained dominated by a single maximum at 0.14 MHz, whereas the STBP spectrum contained two peaks of nearly equal magnitude at 0.27 MHz and 0.49 MHz, where the second peak also existed at 35 mm offset (see Fig. 3a). These STBP peaks occured at larger frequencies than the BP peak, indicating that the STBP had higher frequency content than the BP. On average, the spectra lost approximately 88% ultrasonic energy when the soft tissue was introduced.

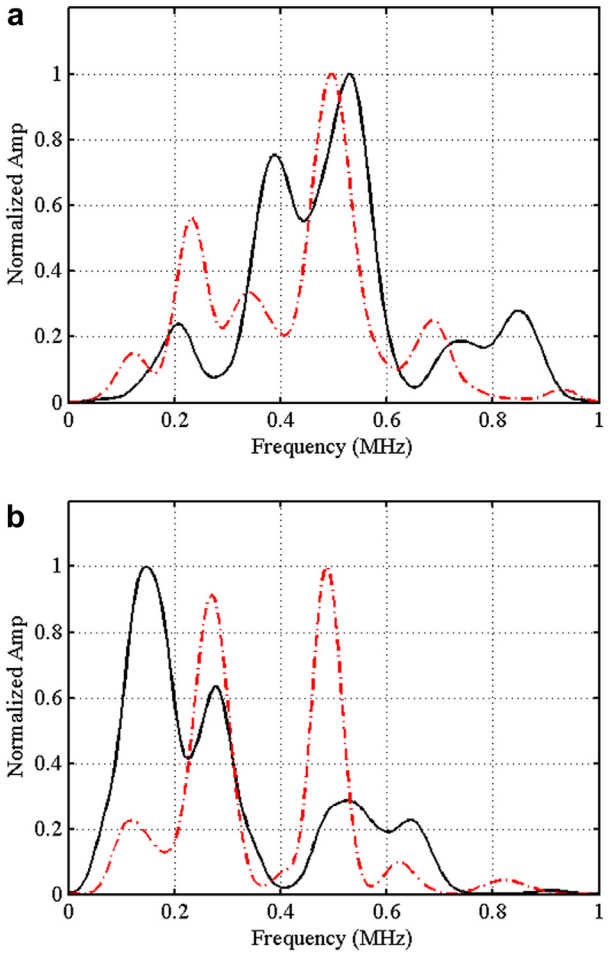

Fig. 3. The amplitude spectra at two offsets: (a) 35 mm and (b) 95 mm. The spectra are self-normalized. The *black solid curve* is for BP and the *red dashed curve* for STBP.

The time-frequency analysis (Fig. 4) indicates the time evolution of the spectral characteristics in the data for the offsets of 35, 55, and 75 mm. Relative to the time record at 35 mm offset, the three time records had the maximum absolute amplitude ratio of 1:0.29:0.14 with corresponding energy ratio of 1:0.14:0.04. The signal strength dropped off considerably with offset. To reveal the presence of low-frequency and low-amplitude signals, the time series were self-normalized before the spectral decomposition analysis. A high-frequency signal dominated the close-offset time record (see Fig. 4a). At mid range, a low-frequency (0.1 MHz) signal began to emerge and attained significant amplitudes at 75 mm offset (see Fig. 4c and d). For STBP, high-frequency signals similar to those of the BP were also identified at 35 mm (see Fig. 4e). This phase group peaked between 0.4 MHz and 0.8 MHz (see also Fig. 3a and b) and remained dominant at longer distances (see Fig. 4f–h). The relative strengths of the high-frequency (0.4–0.8 MHz) and low-frequency (near 0.1 MHz) signals were minimally affected by offset (see Fig. 3a and b), suggesting more high-frequency components than was the case with the BP. Moreover, the STBP had more energy clusters after 50 μs (see Fig. 4c vs. Fig. 4g) than the BP, suggesting more guided modes or enhanced mode density.

To interpret the two bone plate data sets, we computed the theoretical dispersion curves and superimposed the experimental data onto the dispersion map. The experimental data were 2-D–Fourier transformed to the *f-k* domain and then mapped to the f-c_p plane. No significant guided wave energies beyond 0.6 MHz were identified. The maximum intensity loci in the f-c_p panel were determined automatically for a given threshold value and a section of the f-c_p map. The simulated dispersion curves were generated using the commercial software package DISPERSE version 2.0.16i (Imperial College London, London, UK) developed by Pavlakovic and Lowe (2001) and widely used in ultrasonic nondestructive testing. The dispersion curves were calculated using the models with discrete isotropic, homogeneous layers of soft tissue (where applicable) and bone over a water half-space. The thicknesses of modeled layers were relevant to the bovine bone plate and soft-tissue material used in the *in vitro* experiments. The marrow was modeled as a water half-space and the soft tissue was modeled as a solid layer. Following Le et al. (2010), the compressional wave speed, shear wave speed, and density for bone are 4000 m/s, 1970 m/s, and 1930 kg/m^3. Because the symmetric (*S*n) and anti-symmetric (*A*n) modes are reserved for the dry bone plate and the guided modes in a bilayered or multilayered system are no longer

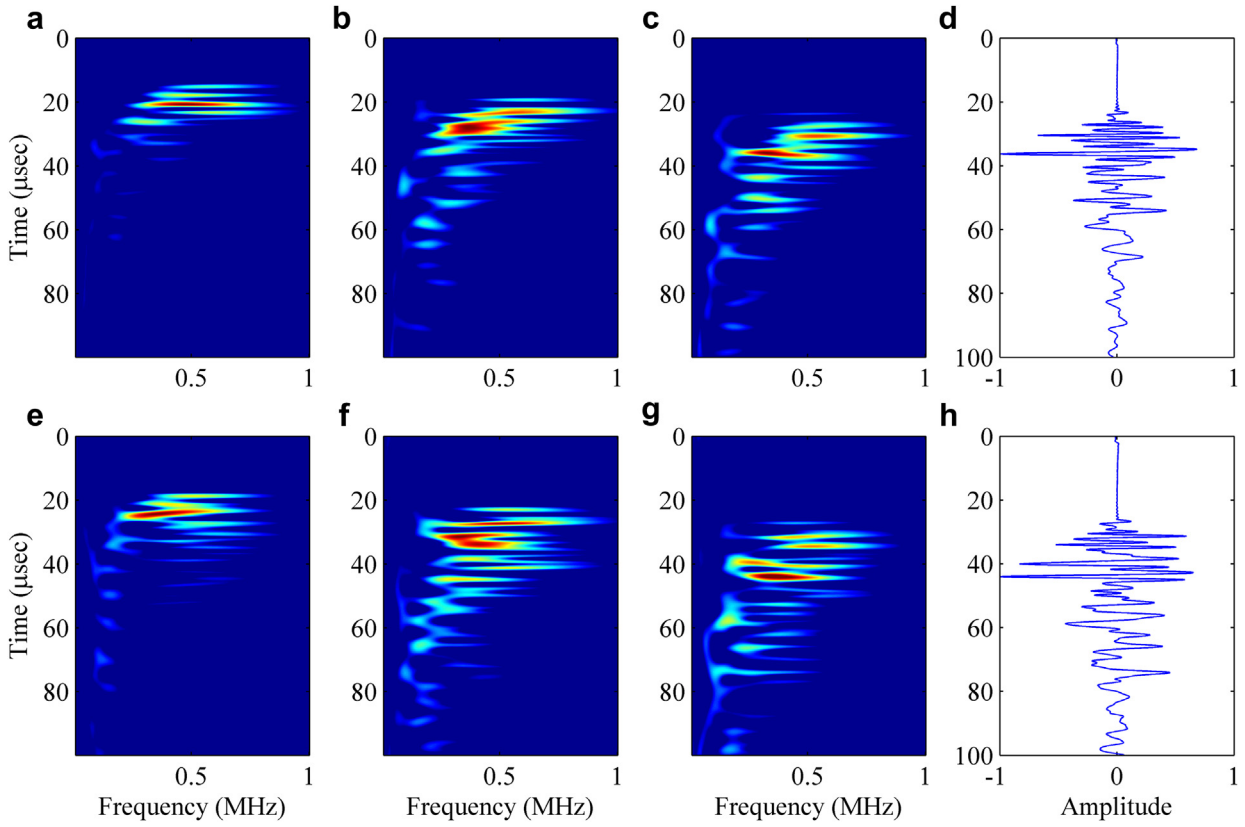

Fig. 4. The *t-f* plots: (a–c) BP; (e–g) STBP. From left to right, the offsets are 35 mm, 55 mm and 75 mm, respectively. Also plotted are the time signals for (d) BP and (h) STBP at 75 mm offset.

standard Lamb modes, we followed Yapura and Kinra (1995) to use ordinal numbers to label guided modes. The dispersion curves for the BP experimental data (Fig. 5a) indicated strong excitations at the leaky Lamb modes 1, 2, 3 and 4. A total of 8 dispersive guided-wave modes (from 1 to 8) were equally well identified in the STBP data (Fig. 5b). The fitting errors between the maximum intensity loci and the predicted dispersive values were calculated for the first two modes. The relative fitting errors (Moilanen et al. 2006) of the BP experimental data were found to be 10.5% and 10.1% for modes 1 and 2, respectively. For the STBP case, the relative fitting errors were 4.9% for mode 1 and 4.3% for mode 2. The experimental data and the theoretical prediction were in close agreement, and elastic models were sufficient for dispersion curve estimation.

DISCUSSION

The main objective of the present study was to investigate the effect of soft tissue on the propagation of ultrasound in long bone. The choice of a bone plate facilitated our analysis of guided modes in plate and effectively eliminated complex cylindrical modes commonly associated with tubular structures. Modal variations of guided waves in a bone plate with and without a soft-tissue mimic were tightly constrained through an integrated analysis involving travel times, temporal-spectral analysis, and dispersion characteristics.

We identified two wave packets (Lee and Yoon 2004; Moilanen et al. 2008; Nicholson et al. 2002) in the experimental data with and without soft-tissue mimic (see Fig. 2). The fast-traveling, high-frequency wave packet was non-dispersive and mainly consisted of reflections, mode conversions, and multiples within the cortex (Le et al. 2010). The arrival times of the various embedded phases were strongly sensitive to small perturbations in compressional and shear wave speeds. The slow-moving wave packet was strongly dispersive and contained significant low-frequency signals, which was particularly evident in the data. Surface waves are known to be dispersive because of variations in the penetrating depths of different frequency components within vertically stratified layers (Aki and Richards 2002; Boiero and Socco 2010; Carannante and Boschi 2005; Knopoff 1972; Rapine et al. 2003; Tatham 1975). For finite values of the ratio between wavelength and plate thickness, Lamb waves can also undergo dispersion similar to surface waves (Cheeke 2002; Rose 1999; Viktorov 1967).

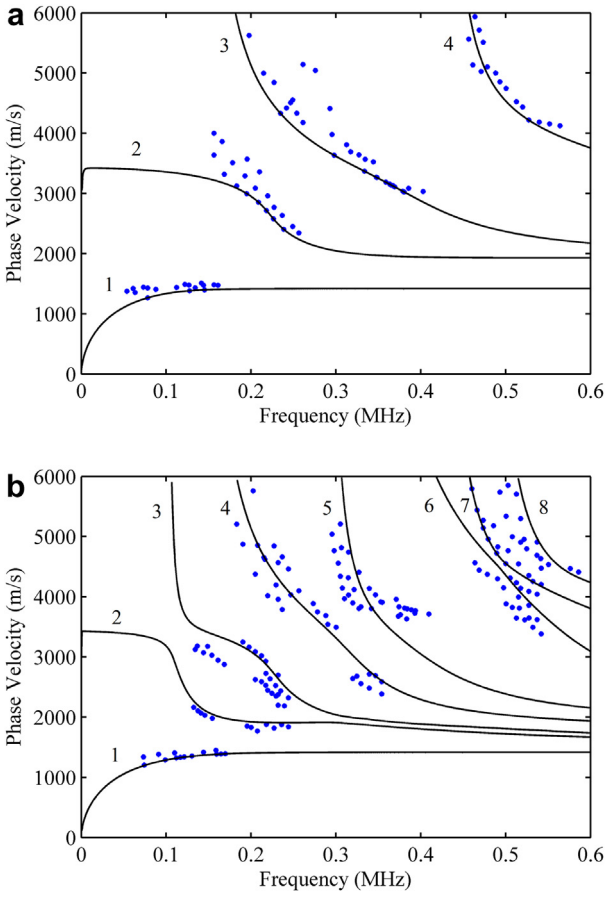

Fig. 5. The theoretical *f-c* dispersion curves for (a) BP and (b) STBP. Superimposed are the maximum intensity loci from the experimental data (*blue dots*).

The introduction of the soft-tissue mimic reduced the recorded ultrasound energy significantly but enhanced the high-frequency contribution to the data. The spectra for BP and STBP were similar at 35 mm offset (see Fig. 3a), though the STBP spectrum skewed toward higher frequencies at far offsets (see Fig. 3b). Further away from the source, the low-frequency signals were observed around 0.1 MHz, with the BP peak much stronger than the STBP peak. The strong high-frequency signals were also present between 0.4 and 0.8 MHz in both cases, but in comparison, the high-frequency components of the STBP spectrum were much stronger than those of the BP spectrum, implying the existence of more high-frequency guided waves in the STBP data. This was supported by the dispersion data (see Fig. 5), which indicated more high-frequency modes were excited in the STBP (see Fig. 5b) than in the BP (see Fig. 5a). These high-order modes traveled with phase velocities over 4000 m/s, similar to the observations reported in previous studies (Lefebvre et al. 2002; Ta et al. 2009). This effect of soft tissue was further evidenced by the *t-f* analysis because the offsets of the high-frequency STBP data (see Fig. 4e–g) exhibited clear correlations with those of bulk-wave phases in BP (see Fig. 4a). The high-frequency phase produced large-amplitude oscillations that persisted at far offsets, and the traveling time was linear with offset (see Fig. 2). Bulk waves were viable candidates considering their short periods and non-dispersive characteristics. The extended wave train could have resulted from the *PP*- and *PS*-reflections and multiples within the cortex (Le et al. 2010). Because the thickness (4 mm) of the soft-tissue layer was larger than the compressional wavelength (1.56 mm), the support of a transient *P* wave within the soft tissue was possible. Because $v_{P,\text{soft tissue}} < v_{S,\text{bone}}$, the lateral shear wave traveling through the soft tissue as compressional wave and horizontally through bone as shear wave was also possible (line B in Fig. 2). At far offsets such as 75 and 95 mm, the timing of the compressional waves traveling from the transmitter to the receivers within the soft-tissue-mimicking layer approximately divided the short-period and long-period zones in the STBP data (line C in Fig. 2). After the arrival of this phase were the *PP*-reflections and their multiples within the soft tissue. These were short-period phases arriving in the long-period and low-speed zone, creating high-frequency fluctuations in the long-period waveforms as a result of their interference. The arrivals of these low-speed and high-frequency phases in the guided-wave regime could adversely affect the delineation of travel-time moveout curves and thereby might lead to erroneous interpretations of the medium properties such as velocity and attenuation.

Guided modes propagating through a material are defined as symmetric or anti-symmetric depending on the particle motion through the plate. For a symmetric mode, particle motion is symmetric across the thickness of the plate and the retrograde elliptical motion at the plate surface is parallel to the direction of propagation (Cheeke 2002; Rose 1999). Anti-symmetric mode exhibits particle motion that is anti-symmetric along the plate thickness and the retrograde elliptical motion at the plate surface is perpendicular to the propagation direction. Lamb waves are waves traveling in a plate bounded above and below by vacuum. With the water half-spaces loading on both sides of the plate, radiation of energy into the surrounding fluid occurs and guided-wave energy, which must travel or "leak" through the water to reach the receivers, is attenuated (Rose 1999). In the present study, the BP and STBP overlaid the water half-space. Energy leakage through the underlying water was possible. Ta et al. (2006, 2009) commented that the presence of overlying soft tissue might cause the drop in detected amplitudes of guided waves because of energy leakage. Yapura and Kinra (1995) studied the characteristic equations and displacement profiles for

a fluid-solid bilayer system immersed in air. In this model, energy leakage does not exist. The displacement profiles determine the measured displacement amplitudes on the surface. In our study, the soft-tissue mimic was a solid layer and displacement amplitudes were considerably different for the BP and STBP when comparing the surface measurements. We think studying the displacement profiles for the two models (BP and STBP) will shed light in explaining the difference in detected amplitudes.

Our experiments provided clear evidence for the existence of mode 1 and mode 2 in BP. These two modes have very similar dispersion characteristics to anti-symmetric *A*0 and symmetric *S*0 Lamb modes in dry plate. Mode 1 was the dominant mode responsible for the strong, late-arriving guided waves at approximately 0.1 MHz (see Fig. 3, Fig. 4c, and Fig. 5a), which is consistent with earlier reports by Nicholson et al. (2002), Dodd et al. (2006), and Moilanen et al. (2006) as an easily detectable guided mode. This mode 1 is also similar to a flexural wave mode as noted by Graff (1991) and Nicholson et al. (2002).

The dispersion curves changed considerably when soft tissue was introduced to the model. Modes tended to cluster and mode density increased, results consistent with findings by Moilanen et al. (2006, 2008) using numerical simulation for a bilayered fluid-solid tube model and with phantom study by Chen et al. (2012). The number of guided modes also increased and more high-frequency and high-speed modes were detectable (see Fig. 5b). Of the detectable leaky modes, mode 1 was minimally affected by the addition of soft tissue; a similar effect was previously documented for a plate immersed in water (see Moilanen et al. 2006 and Dodd et al. 2006). Although the multiplicity of high-frequency modes accentuates the inherent complexities of *in vivo* analyses, it also presents future additional observational constraints on osteoporosis.

One key contribution of this study is a successful attempt to mimic real long bone with a bovine bone plate and soft-tissue mimic, which, in density, attenuation, compressional wave speed and shear wave speed, resembled real soft tissue, and to analyze the data using travel times, spectral analysis, time frequency map, and dispersion-curve calculation based on a simplistic, horizontally stratified model containing three layers. The work is a step forward from phantom work to close-to-real clinical measurements. We attempted to analyze the data using both the ray and wave concepts. The interpretations are not in conflict but complement each other, leading to a fruitful discussion. For example, the direct *P, PP*-reflections and the multiples within the soft tissue had high frequencies and low speeds. Although their presence in the low-velocity guided-wave zone could be predicted by the arrival times, they were not shown in the dispersion map, perhaps because of their small amplitudes. It is uncertain whether these compressional bulk phases in the low-velocity guided-wave regime are important; however, their interaction with the long-period wave trains created some subtle high-frequency oscillations in the STBP data compared with the BP data. The combined analytical method not only provides an effective tool to verify key guided-wave signals contained in the experimental data but also provides a roadmap for revealing the nature of the complex interaction between ultrasound waves and soft-tissue/bone structures. Future study of the effect of soft-tissue thickness on the generation of guided waves will be beneficial to advance this study further.

CONCLUSIONS

In this paper, we reported that the presence of a soft-tissue layer affects the behavior of guided waves in long bone. By adopting a 4-mm mimic with similar material properties to those of soft tissue and using a combination of travel times, dispersion-curve computation, and time-frequency analysis, we were able to not only observe both bulk (compressional and shear) and guided waves but also identify the individual guided modes that were responsible for these oscillations. For STBP, the additional soft tissue attenuated the ultrasound signals significantly and increased the number of guided modes and mode density. Besides material absorption of the soft tissue, the displacement profiles of the BP and STBP might be the major determinant for the detected amplitudes on the surface based on a bilayer system. Guided modes were identified in the f-c_p domain, and their dispersion characteristics were consistent with theoretical predictions. The signals had larger high-frequency content compared with no soft-tissue signals. The addition of t-f analysis and simple travel-time calculation enabled us to reveal the presence of bulk waves in soft tissue and their presence in the low-velocity guided wave regime. Our integrated approach could provide a promising blueprint for future *in vivo* studies of human tibia.

Acknowledgments—The authors thank David Bonar for discussion of and assistance with spectral decomposition and Alex Tsang for data acquisition. We acknowledge valuable discussion with Professors Yang Che-Hua and Wu Chia-Han about guided-wave dispersion. This work was supported by a university graduate scholarship (T.T.), a NSERC postgraduate scholarship (L.S.) and a Discovery Grant from the National Science and Engineering Research Council of Canada.

REFERENCES

Aki K, Richards PG. Quantitative seismology. 2nd edition. South Orange, NJ: University Science Books; 2002.

Alleyne D, Cawley P. A two-dimensional Fourier transform method for the measurement of propagating multimode signals. J Acoust Soc Am 1991;89:1159–1168.

Boiero D, Socco L. Retrieving lateral variations from surface wave dispersion curves. Geophys Prospect 2010;58:977–996.
Bonar DC, Sacchi MD. Complex spectral decomposition via inversion strategies. SEG Technical Program Expanded Abstracts 2010;29: 1408–1412.
Bossy E, Talmant M, Defontaine M, Patat F, Laugier P. Bidirectional axial transmission can improve accuracy and precision of ultrasonic velocity measurement in cortical bone: A validation on test materials. IEEE Trans Ultrason Ferroelectr Freq Control 2004a; 51:71–79.
Bossy E, Talmant M, Laugier P. Three-dimensional simulations of ultrasonic axial transmission velocity measurement on cortical bone models. J Acoust Soc Am 2004b;115:2314–2324.
Carannante S, Boschi L. Databases of surface wave dispersion. Ann Geophys 2005;48:945–955.
Cheeke JDN. Fundamentals and applications of ultrasonic waves. Boca Raton, FL: CRC Press; 2002.
Chen J, Foiret J, Minonzio JG, Talmant M, Su Z, Cheng L, Laugier P. Measurement of guided mode wavenumbers in soft tissue-bone mimicking phantoms using ultrasonic axial transmission. Phys Med Biol 2012;57:3025–3037.
Culjat M, Goldenberg D, Tewari P, Singh R. A review of tissue substitutes for ultrasound imaging. Ultrasound Med Biol 2010;36: 861–873.
Dodd SP, Cunningham JL, Miles AW, Gheduzzi S, Humphrey VF. Ultrasonic propagation in cortical bone mimics. Phys Med Biol 2006;51: 4635–4647.
Frizzell LA, Carstensen EL, Dyro JF. Shear properties of mammalian tissues at low megahertz frequencies. J Acoust Soc Am 1976;60: 1409–1411.
Gerlanc M, Haddad D, Hyatt GW, Langloh JT, Hilaire PS. Ultrasonic study of normal and fractured bone. Clin Orthop Relat Res 1975;175–180.
Graff KF. Wave motion in elastic solids. New York: Dover; 1991.
Knopoff L. Observation and inversion of surface-wave dispersion. Tectonophysics 1972;13:497–519.
Laugier P. Quantitative ultrasound of bone: looking ahead. Joint Bone Spine 2006;73:125–128.
Le LH, Gu YJ, Li Y, Zhang C. Probing long bones with ultrasonic body waves. Appl Phys Lett 2010;96.
Lee KI, Yoon SW. Feasibility of bone assessment with leaky lamb waves, in bone phantoms and a bovine tibia. J Acoust Soc Am 2004;115:3210–3217.
Lefebvre F, Deblock Y, Campistron P, Ahite D, Fabre JJ. Development of a new ultrasonic technique for bone and biomaterials in vitro characterization. J Biomed Mater Res 2002;63:441–446.
Lowet G, der Perre GV. Ultrasound velocity measurement in long bones: Measurement method and simulation of ultrasound wave propagation. J Biomech 1996;29:1255–1262.
Madsen EL, Sathoff HJ, Zagzebski JA. Ultrasonic shear wave properties of soft tissues and tissuelike materials. J Acoust Soc Am 1983;74: 1346–1355.
Madsen EL, Zagzebski JA, Banjavie RA, Jutila RE. Tissue mimicking materials for ultrasound phantoms. Med Phys 1978;5:391–394.
Moilanen P. Ultrasonic guided waves in bone. IEEE Trans Ultrason Ferroelectr Freq Control 2008;55:1277–1286.
Moilanen P, Nicholson PHF, Kilappa V, Cheng S, Timonen J. Measuring guided waves in long bones: Modeling and experiments in free and immersed plates. Ultrasound Med Biol 2006;32:709–719.
Moilanen P, Talmant M, Kilappa V, Nicholson P, Cheng S, Timonen J, Laugier P. Modeling the impact of soft tissue on axial transmission measurements of ultrasonic guided waves in human radius. J Acoust Soc Am 2008;124:2364–2373.
Muller M, Moilanen P, Bossy E, Nicholson P, Kilappa V, Timonen J, Talmant M, Cheng S, Laugier P. Comparison of three ultrasonic axial transmission methods for bone assessment. Ultrasound Med Biol 2005;31:633–642.
Nicholson PHF, Moilanen P, Karkkainen T, Timonen J, Cheng SL. Guided ultrasonic waves in long bones: Modelling, experiment and in vivo application. Physiol Meas 2002;23:755–768.
Njeh C, Boivin C, Langton C. The role of ultrasound in the assessment of osteoporosis: A review. Osteoporosis Int 1997;7:7–22.
Pavlakovic B, Lowe M. DISPERSE user's manual, version 2.0. London: Imperial College; 2001.
Prosser W, Seale M, Smith B. Time-frequency analysis of the dispersion of lamb modes. J Acoust Soc Am 1999;105:2669–2676.
Rapine R, Tilmann F, West M, Ni J, Rodgers A. Crustal structure of northern and southern tibet from surface wave dispersion analysis. J Geophys Res-Sol Ea 2003;108.
Reginster J, Burlet N. Osteoporosis: A still increasing prevalence. Bone 2006;38:4–9.
Rose JL. Ultrasonic waves in solid media. New York: Cambridge University Press; 1999.
Ryan H Ricker. Ormsby, Klauder, Butterworth—a choice of wavelets. CSEG Recorder 1994;19:8–9.
Siegel I, Anast G, Fields T. The determination of fracture healing by measurement of the sound velocity across the fracture side. Surg Gynec Ostet 1958;107:327–332.
Ta D, Huang K, Wang W, Wang Y, Le LH. Identification and analysis of multimode guided waves in tibia cortical bone. Ultrasonics 2006;44: E279–E284.
Ta D, Wang W, Wang Y, Le LH, Zhou Y. Measurement of the dispersion and attenuation of cylindrical ultrasonic guided waves in long bone. Ultrasound Med Biol 2009;35:641–652.
Tatarinov A, Sarvazyan N, Sarvazyan A. Use of multiple acoustic wave modes for assessment of long bones: Model study. Ultrasonics 2005; 43:672–680.
Tatham R. Surface-wave dispersion applied to detection of sedimentary basins. Geophysics 1975;40:40–55.
Vavva MG, Protopappas VC, Gergidis LN, Charalambopoulos A, Fotiadis DI, Polyzos D. The effect of boundary conditions on guided wave propagation in two-dimensional models of healing bone. Ultrasonics 2008;48:598–606.
Viktorov IA. Rayleigh and Lamb waves. New York: Plenum Press; 1967.
Werner P. Knowledge about osteoporosis: assessment, correlates and outcomes. Osteoporosis Int 2004;16:115–127.
Xu K, Ta D, Wang W. Multiridge-based analysis for separating individual modes from multimodal guided wave signals in long bones. IEEE Trans Ultrason Ferroelectr Freq Control 2010;57: 2480–2490.
Yapura CL, Kinra VK. Guided waves in a fluid-solid bilayer. Wave Motion 1995;21:35–46.
Zhang M, Castaneda B, Wu Z, Nigwekar P, Joseph JV, Rubens DJ, Parker KJ. Congruence of imaging estimators and mechanical measurements of viscoelastic properties of soft tissues. Ultrasound Med Biol 2007;33:1617–1631.
Zhao Z, Moilanen P, Karppinen P, Maatta M, Karppinen T, Haggstrom E, Timonen J, Myllyla R. Photo-acoustic excitation and detection of guided ultrasonic waves in bone samples covered by a soft coating layer. Proc of SPIE 2012;8553: 85531.E1–85531.E8.